

SANDIA REPORT

SAND97-8246 • UC-706

Unlimited Release

Printed March 1997

Characterization and Electrical Modeling of Semiconductor Bridges

K. D. Marx, R. W. Bickes, Jr., and D. E. Wackerbarth

Prepared by
Sandia National Laboratories
Albuquerque, New Mexico 87185 and Livermore, California 94551
for the United States Department of Energy
under Contract DE-AC04-94AL85000

Approved for public release; distribution is unlimited.

Issued by Sandia National Laboratories, operated for the United States Department of Energy by Sandia Corporation. NOTICE: This report was prepared as an account of work sponsored by an agency of the United States Government. Neither the United States Government nor any agency thereof, nor any of their employees, nor any of the contractors, subcontractors, or their employees, makes any warranty, express or implied, or assumes any legal liability or responsibility for the accuracy, completeness, or usefulness of any information, apparatus, product, or process disclosed, or represents that its use would not infringe privately owned rights. Reference herein to any specific commercial product, process, or service by trade name, trademark, manufacturer, or otherwise, does not necessarily constitute or imply its endorsement, recommendation, or favoring by the United States Government, any agency thereof or any of their contractors or subcontractors. The views and opinions expressed herein do not necessarily state or reflect those of the United States Government, any agency thereof, or any of their contractors or subcontractors.

This report has been reproduced from the best available copy.

Available to DOE and DOE contractors from:

Office of Scientific and Technical Information
P.O. Box 62
Oak Ridge TN 37831

Prices available from (615) 576-8401, FTS 626-8401.

Available to the public from:

National Technical Information Service
U.S. Department of Commerce
5285 Port Royal Rd.
Springfield, VA 22161

SAND97-8246
Unlimited Release
Printed March 1997

CHARACTERIZATION AND ELECTRICAL MODELING OF SEMICONDUCTOR BRIDGES

K. D. Marx*, R. W. Bickes, Jr.†, and D. E. Wackerbarth†

**Sandia National Laboratories
*Livermore, California
and
†Albuquerque, New Mexico**

Abstract

Semiconductor bridges (SCBs) are finding increased use as initiators for explosive and pyrotechnic devices. They offer advantages in reduced voltage and energy requirements, coupled with excellent safety features. The design of explosive systems which implement either SCBs or metal bridgewires can be facilitated through the use of electrical simulation software such as the PSpice® computer code. A key component in the electrical simulation of such systems is an electrical model of the bridge. This report has two objectives: (1) to present and characterize electrical data taken in tests of detonators which employ SCBs with BNCP as the explosive powder; and (2) to derive appropriate electrical models for such detonators. The basis of such models is a description of the resistance as a function of energy deposited in the SCB. However, two important features which must be added to this are (1) the inclusion of energy loss through such mechanisms as ohmic heating of the aluminum lands and heat transfer from the bridge to the surrounding media; and (2) accounting for energy deposited in the SCB through heat transfer to the bridge from the explosive powder after the powder ignites. The modeling procedure is entirely empirical; i.e., models for the SCB resistance and the energy gain and loss have been estimated from experimental data taken over a range of firing conditions. We present results obtained by applying the model to the simulation of SCB operation in representative tests.

I. Introduction

The purpose of this report is to provide some recent data from detonators which employ semiconductor bridges (SCBs), and to present a model which can be used in the electrical simulation of such detonators. The operating principles of SCBs and their application in explosive devices are discussed in Benson, et al., (1987), Bickes, et al., (1988), Martínez Tovar, (1993), and Bickes, et al., (1995).

An SCB (see Figure 1) consists of a small doped polysilicon volume formed on a silicon substrate. The length of the bridge (100 μm) is determined by the spacing of the aluminum lands seen in the figure. The doped layer is 2 μm thick, and the bridge is 380 μm wide. The lands provide a low ohmic contact to the underlying doped layer. Wires ultrasonically bonded to the lands permit a current pulse to flow from land to land through the bridge. The current pulse through the SCB causes it to burst into a bright plasma discharge that heats the exoergic powder pressed against it by a convective process that is both rapid and efficient. Consequently, SCB devices operate at very low energies and function very quickly. But despite the low energy for ignition, the substrate provides a reliable heat sink for excellent no-fire levels.

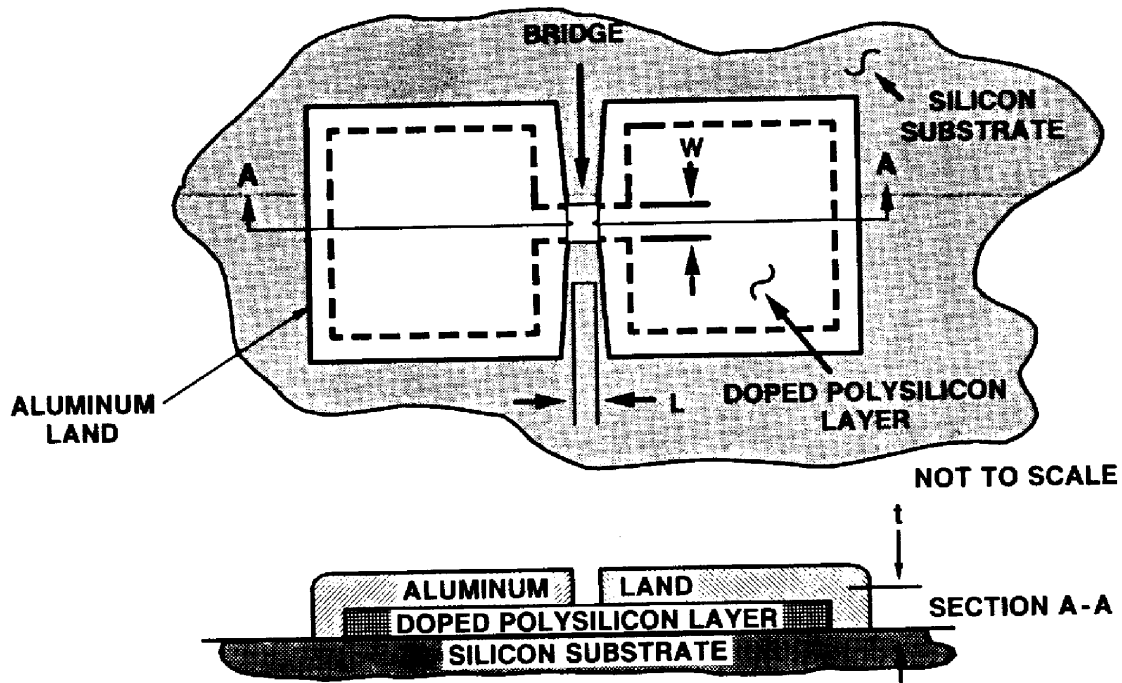


Figure 1. Simplified sketch of a semiconductor bridge (SCB). The bridge is formed from the heavily doped polysilicon layer enclosed by the dashed lines. Bridge dimensions are 380 μm wide (W) by 100 μm long (L) by 2 μm thick (t). Electrical leads are attached to the aluminum lands permitting an applied current pulse to flow from land to land through the bridge.

The detonator used for the experiments in this report is shown in Figure 2. Type 3-2B1 die were mounted on standard TO-46 transistor headers; bridge dimensions were 100 μm long and 380 μm wide. The charge holder was a brass cylinder pressed and glued onto the TO-46 header. The devices were loaded with 75 mg of BNCP[†] that was pressed against the SCB at 20,000 psi. The BNCP was processed by Pacific Scientific, Chandler, Arizona.

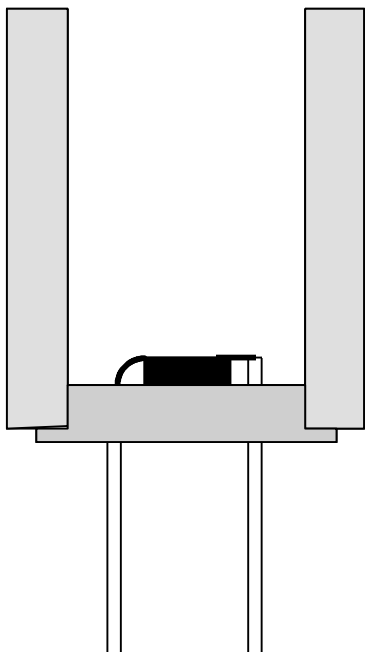


Figure 2. TO-46 transistor base with a brass charge holder. The internal diameter of the charge holder is 0.150" (3.8 mm) and the internal length is 0.270" (6.9 mm). The outside diameter of the charge holder is 0.25" (6.4 mm). Seventy-five milligrams of BNCP is poured into the charge holder and then pressed at 20,000 psi against the SCB.

The electrical data that we present here provides some new insights into the way that SCBs operate in a detonator, particularly with respect to the interaction of the explosive powder and the SCB. We will show that it is important to include this interaction in the electrical model of the detonator. Tests of SCBs firing in air and into various explosive powders have shown that the electrical behavior of the SCB is very dependent on the presence or absence of the powder, and on the type of powder used. For example, THKP* is more electrically conductive than BNCP, and the impedance seen by a firing set driving an SCB/THKP ignitor is significantly lower than is the case for either an SCB/BNCP detonator or an SCB fired in air. For this reason, it would be an extensive project to try to characterize and model SCBs in many such configurations. We elected to restrict this work to the case of BNCP powder.

The reasons for developing detonator models are the same as those for obtaining models for any electrical components. Given an accurate detonator model and models for all the other electrical components in a firing system, one can (1) optimize the design of the firing system with a minimum of laboratory testing; and (2) estimate the effects on the system due to the failure of components or the deviation from specification of components for any reason, such as aging or temperature extremes.

A great deal of effort has been put into the development of models for exploding bridgewires (EBWs) and exploding foils (Furnberg, 1994). That work has been very successful and has provided the explosives community with useful tools for the design and

[†] Tetraamminebis (5-nitro-2H-tetrazolato-N²) cobalt(III) perchlorate.

* Titanium subhydride potassium perchlorate.

analysis of explosive systems. The basis of those models is a description of the detonator resistance as a function of energy. We adopted this approach and added empirical descriptions of SCB energy loss and the feedback of thermal energy from the explosive powder to the SCB. This was found to be necessary in order to describe the interaction between the SCB and its surroundings.

In this report, detonator models consist of the mathematical and computational specification of the electrical behavior of the detonator, and as such, will be independent of any particular simulation software tool. However, we used exclusively the PSpice® computer program developed and marketed by MicroSim® Corporation. The mathematical models were implemented through the use of the Analog Behavioral Modeling feature in PSpice. Although not explicitly stated, this may be assumed in the specific model development and subsequent calculations discussed here.

In the following section, the approach used to model EBWs is described, and an SCB model based on that approach is derived. We will demonstrate that this model has applicability over a limited range of firing set voltages and energies. In the next section, SCB detonator data taken over a broad range of voltages and energies is presented and interpreted in terms of the SCB energy budget. This will lead to the introduction of models for energy loss and for thermal feedback from the explosive powder. These models were implemented into our overall SCB/BNCP models and comparisons between simulations using these models and experimental data are given in Section III.

II. Basic Approach to Characterization and Modeling of SCBs

As our modeling of SCBs has borrowed heavily from that used for EBW devices, we first give a very brief review of the procedures employed for those studies.

Exploding Bridgewires (EBWs)

The electrical response of an EBW is characterized by the following behavior: (1) when the deposit of electrical energy into the bridge is initiated, there is an increase in resistance at early times up to some peak value; (2) this is followed by a drop in resistance down to some value which remains roughly constant over times of interest (see Furnberg, 1994 and Figure 3). The initial rise is due to the positive temperature coefficient of resistivity of metals from ambient temperatures up to the point of vaporization. The peak value of resistance corresponds to bridgewire burst, and the time at which the peak occurs is defined as the burst time. The drop in resistance and approach to a plateau corresponds to the decrease in resistivity incurred as the metal vaporizes and then partially ionizes.

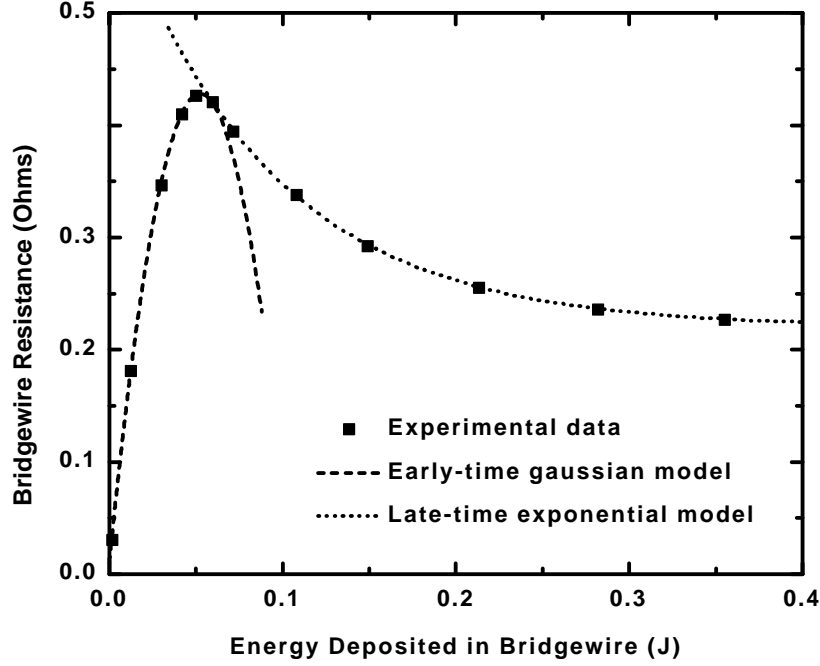


Figure 3. Data typical of exploding bridgewires (EBWs). Time histories of voltage and current are used to obtain the energy and resistance as a function of time from Eqs. (1) and (2). These results are then combined in the plot shown. The gaussian and exponential curve fits used in the EBW model (see text) are superimposed on the plot.

This behavior is modeled by an approach which is primarily based on the assumption that the resistance is a unique function of the energy E delivered to the bridge-wire, given by

$$E = \int_0^t VI dt, \quad (1)$$

where V is voltage across the bridgewire leads, I is current through the bridgewire, and t is time. Bridgewire resistance is simply defined as

$$R = V/I. \quad (2)$$

Another quantity which is useful in interpreting EBW behavior is the action,

$$A = \int_0^t I^2 dt. \quad (3)$$

It is found that the best EBW models make a slight compromise in the reproduction of the dependence of resistance on energy in order to accommodate the observation that the best agreement with experiment is obtained when the model is adjusted so that the action at burst agrees with the experimental value.

To obtain a PSpice model of an EBW, an experimentally measured resistance versus energy plot is fit to two overlapping mathematical functions (see Figure 3): (1) a gaussian to describe the initial rise and the very early part of the drop in resistance; and (2) an exponential decay to the late-time plateau. There are 7 parameters which define these functions. Some of these parameters are determined by imposing various constraints involving resistance values, action to burst, and continuity. These constraints uniquely determine the gaussian function. The remaining parameters determine the decay rate and late-time value of the exponential, and are adjusted visually for an optimal fit to the data. The gaussian and exponential functions are then employed in a PSpice model to specify the instantaneous resistance of the device in circuit simulations.

Semiconductor Bridges: Simple Model

Data from a typical SCB shot are shown in Figure 4. The firing set used for this test contained a 19.08 μF capacitor charged to 50 V. (Table I provides information on all the SCB tests to be discussed in this report. For future reference, we note that the data in Figure 4 are from Shot #1318, and that the shortest possible cable connection was used between the output of the firing set and the SCB.) Note the sudden drop in current and the rise in voltage at approximately 1.6 μs . This corresponds to vaporization of the bridge, and the time at which this occurs is denoted as burst time in the figure. Throughout this report, burst time will be defined as the time of the beginning of the current drop.

Unpublished experiments with THKP actuators and a crowbar firing set demonstrated that vaporization of the bridge was required to obtain ignition of the THKP. When the current was turned off (crowbarred) at any time prior to the burst time, the actuator did not function. In contrast, if the current was turned off after the burst time the unit still functioned. We believe that vaporization of the bridge is also required for BNCP; however, crowbar BNCP experiments have not been carried out as yet.

Note from the resistance plot that the ratio of voltage to current is very large at very early times. This is not true resistance; the initial SCB resistance is approximately 1 Ω , and it is expected that the resistance increases monotonically to the first peak shown at approximately 0.6 μs . The large ratio of voltage to current is due to inductance in the circuit and is just an initial transient that always appears in the very early data.

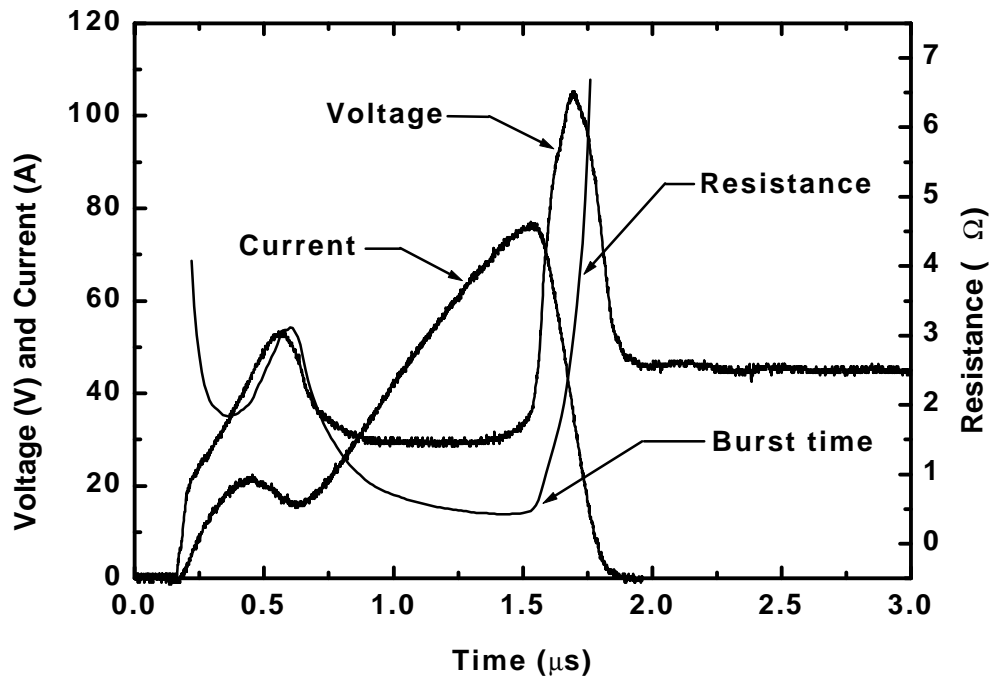


Figure 4. Data from SCB Shot #1318 illustrating standard behavior. Raw data are shown for the voltage and current; however, the resistance is obtained from filtered voltage and current signals.

The resistance versus energy plot resulting from the data in Figure 4 is shown in Figure 5. This is what one might refer to as “classic” SCB data. The various regions of silicon conduction are indicated. The bridge proceeds through the following stages: (1) extrinsic conduction, when the silicon exhibits a positive temperature coefficient of resistivity; (2) intrinsic conduction, when the temperature of the bridge is raised sufficiently to release a large number of charge carriers, and the temperature coefficient of resistivity is negative; (3) melt, and (4) vaporization, when the resistivity of the silicon increases rapidly. The dashed line denoted “true” simply indicates the approximate resistance behavior of the bridge at early times, as discussed previously.

We note that burst occurs at about 1.7 mJ. The enthalpy required to completely vaporize the silicon in the bridge was calculated to be 1.65 mJ, of which 1.1 mJ is required for vaporization with the remainder used for heating and melting. (The difference between enthalpy and energy is of the order of 0.1 mJ, and may be ignored.) Hence, we can say that the theoretical order of magnitude of the energy to burst is reflected in the data. However, we do not believe that vaporization is complete at the point that we have defined as burst. Therefore, the apparent agreement between the values of 1.7 mJ and 1.65 mJ is fortuitous; there is some energy loss. We note that the

Table I. Semiconductor bridge tests discussed in this report. The CDU energies and voltages are somewhat loosely categorized into low, intermediate, and high. (In the present work, high voltage is a relative term, and does not imply kilovolts.) At high voltage, the behavior of the SCBs appears to be dominated by the voltage. For example, Shot #1333 at 90V behaves more like Shot #1322 (90 V) than like #1318 (50 V), even though the energy in #1333 (13.7 mJ) is lower than that of #1318 (23.9 mJ). See Figures 13 and 14.

Shot Number	Capacitance (μF)	CDU Voltage (V)	Energy E_o (mJ)	Comments
1281	9.57	28	3.75	Long cables, low energy/voltage
1294	9.57	28	3.75	Long cables, low energy/voltage, like 1281
1299	19.08	50	23.9	Long cables, intermediate energy/voltage
1300	19.08	50	23.9	Long cables, intermediate energy/voltage, like 1299
1316	10.34	28	4.07	Low energy/voltage
1317	19.08	50	23.9	Intermediate energy/voltage
1318	19.08	50	23.9	Intermediate energy/voltage, like 1317
1322	10.34	90	41.9	High energy/voltage
1323	10.34	70	24.5	Intermediate energy, high voltage
1324	23.2	70	56.8	High energy/voltage
1325	23.2	70	56.8	High energy/voltage, like 1324
1330	3.38	70	8.3	Intermediate energy, high voltage
1331	38.1	70	93.3	High energy/voltage
1332	38.1	90	154.3	High energy/voltage
1333	3.38	90	13.7	Intermediate energy, high voltage
1334	3.38	50	4.23	Low energy, intermediate voltage
1335	3.38	28	1.33	Low energy/voltage
1336	10.34	70	24.5	Intermediate energy, high voltage, like 1323
1338	10.34	20	2.07	Low energy/voltage
1339	38.1	20	7.62	Low energy/voltage
1340	38.1	28	14.9	Intermediate energy, low voltage
1341	38.1	15	4.29	Low energy/voltage

initial energy $E_0 = 23.9$ mJ stored on the capacitor is much more than that required to vaporize the bridge.

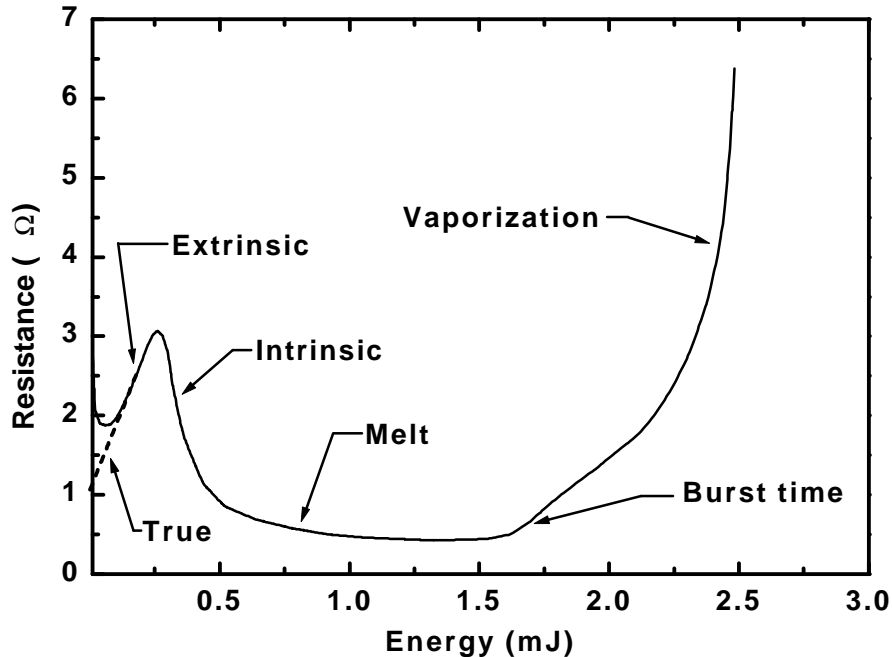


Figure 5. Resistance versus energy taken from the data shown in Figure 4. As indicated in the caption for Figure 4, the resistance and energy are obtained from filtered voltage and current data.

Note that the behavior of the SCB resistance is somewhat more complicated than that of the EBW illustrated in Figure 3. This has a significant effect on the way the SCB model is implemented in comparison to EBW models. Specifically, we used a table lookup procedure in PSpice to model the resistance as a function of energy, rather than a sequence of mathematical functions. We tried the latter initially, but the structure of R vs. E for the SCBs quickly results in too much numerical complexity to be practical.

The procedure for obtaining a simple model for an SCB from the data shown in Figures 4 and 5 is as follows. (1) Obtain a spline fit to the R vs. E data in order to provide additional smoothing. (2) Create a table of R and E values from the fit. And, (3) create a PSpice part which is an analog behavioral model having the R vs. E characteristics given by the table. The Origin™ data analysis software from Microcal Software™ was used for Steps (1) and (2). We used their B-Spline fit in Step (1). The table created in Step (2) from the data of Figure 5 consists of 148 points from 0 to 2.51 mJ.

Results Obtained with the Simple Model

Discussion of the results obtained from this simple model for the SCB will begin with a description of the firing set used to obtain test data from the bridge. The firing set electrical schematic is displayed in Figure 6. The data on which we relied most heavily (the last 18 entries in Table I) were taken with very short wires from the output of the firing set (i.e., from Points 1 and 2 in the figure) to the SCB. An SCB model could be inferred from this data without reference to the firing set. However, the details of the firing set are relevant to the model development for the following reasons: (a) we use a model of the experimental circuit, including the SCB model, to check the accuracy of the SCB model; and (b) some of our data was taken with 18 inches of RG-58 cable and 6 inches of twisted pair 22 gauge wires connecting the bridge to the output of the firing set (e.g., the first four entries in Table I), and it was necessary to take the extra cable length into account in processing the data from these tests.

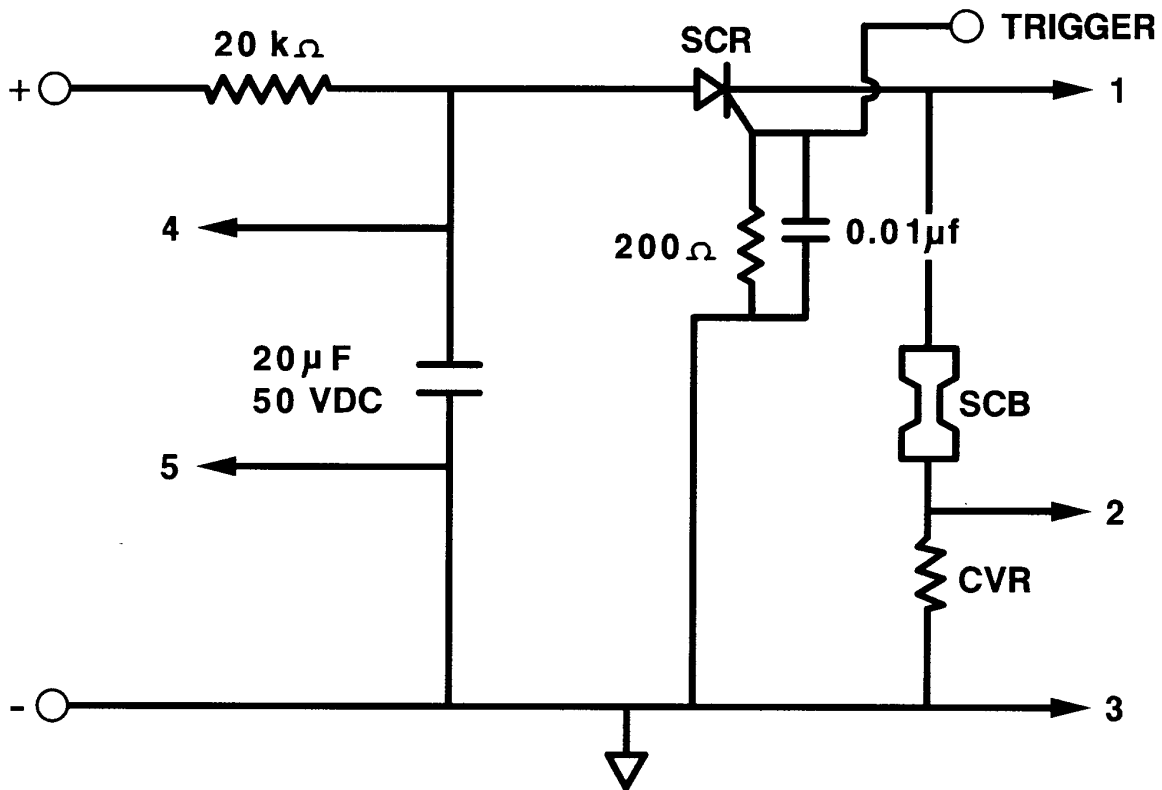


Figure 6. Firing set used for SCB tests. Voltage data is taken from a 50 Ω instrumentation line connected between Points 1 and 3. Current data is taken from a similar line connected between Points 2 and 3. In the present work, the capacitance and initial voltage (shown here as 20 μF and 50 V) were varied between 3.38 μF and 38.1 μF, and between 15 V and 90 V, respectively.

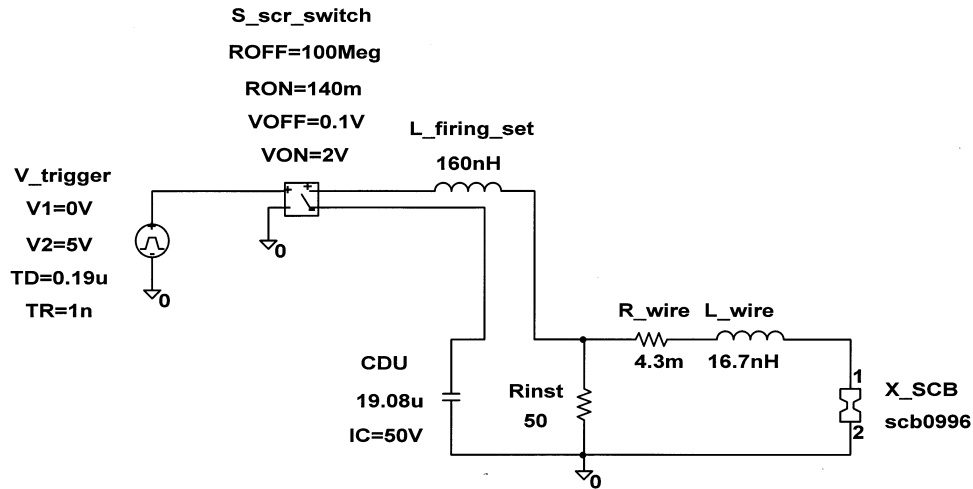


Figure 7. PSPice model for the circuit used to obtain SCB data. The values R_{wire} and L_{wire} shown are estimates for the short cables used (see text). The CVR used to obtain current data (see Figure 6) was not included in the circuit.

We included the early-time impedance measured at Points 1 and 2 in the tabular data used in the model. In other words, we are modeling the initial transient (see discussion above) by including the effects of the impedance of the short wire connections and the SCB itself in the model. This is a weakness of the model, but we believe it is a minor one. We made attempts to model this impedance as a constant inductance and resistance, but this did not prove to be very satisfactory. We assumed that one reason was that the early-time impedance is dominated by the skin effect, and requires a more accurate treatment than time-invariant parameters can provide. We note in passing that the skin-effect impedance involves the square root of the frequency, and that PSPice can accommodate such an impedance. However, our experience indicated that this would increase the computer run time significantly, and we felt that the improvement in accuracy would not justify the additional run time and complexity.

The PSPice schematic of the circuit we used to simulate the SCB tests is shown in Figure 7. Although we tried to use a PSPice SCR model for the SCR switch that was used in the experiment, we found that the model did not simulate the switch closing behavior accurately. Instead, we employed the simple PSPice voltage-controlled switch model shown, which provided adequate results. The 50 Ω voltage instrumentation line was included in the circuit. But the 0.01 Ω CVR and its 50 Ω instrumentation line were not included; the effects of both of these were slight, compared to the effects of inaccuracies in the model. The resistance R_{wire} and inductance L_{wire} shown in the figure are estimates for the lines connecting the firing set to the SCB. They were obtained by scaling the corresponding parameters for 6 inches of twisted pair wire that were used, along with 18 inches of RG-58 cable for some tests (referred to as long-cable tests below). However,

the values of R_{wire} and L_{wire} in the circuit shown in Figure 7 (i.e., in the short-cable tests) had little effect.

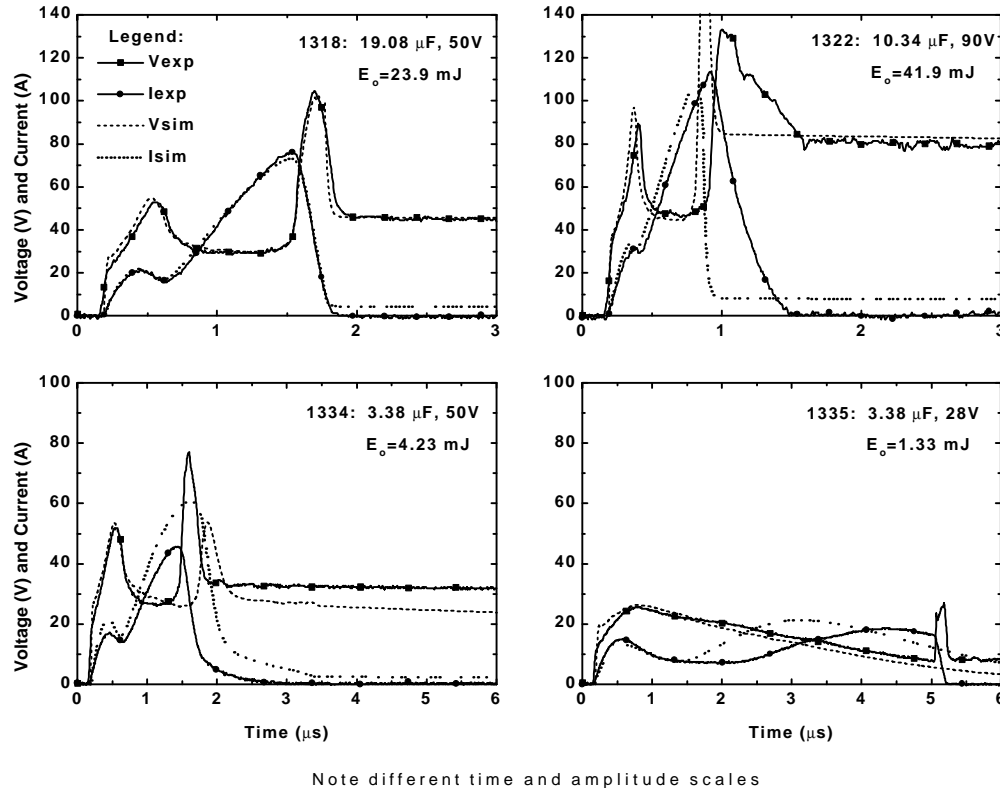


Figure 8. Results of applying the simple SCB model to four tests which differ widely in the energy E_o initially stored on the capacitor discharge unit (CDU). Shot #1318 lies in an intermediate energy range, and yields “classic” SCB behavior. Shot #1332 is in the high energy range. Note that the voltage predicted by the model goes off the scale of the plot—up to more than 700 V. Shots #1334 and 1335 are in the low energy range (see text). In the case of Shot #1335, the simulation does not predict SCB burst—no matter how far out in time the computation is extended. Note: In this figure and all those that follow, the voltage and current data are smoothed by averaging the raw data over 26 neighboring points at each value of time. The raw voltage and current data (shown only in Figure 4) contain points at 1 ns intervals.

Figure 8 gives the results of simulating four different SCB tests with the simple model discussed above. First consider Shot #1318. The agreement with experiment is very good, because this was the test used to derive the model. There is, however, one aspect to this that may not be obvious. The amplitude of the voltage spike at burst depends

very little on the SCB model; it is dominated by the inductance L_{fs} of the firing set (see L_{firing_set} in Figure 7). Ignoring the resistance of the SCR and CVR and any wire resistance, the voltage V_{inst} measured at Point 1 in Figures 6 and 7 is given by

$$V_{inst} = V_C - L_{fs} \frac{dI_{fs}}{dt} \quad (4)$$

where V_C is the instantaneous capacitor voltage and I_{fs} is the current in the firing set. Given the correct R vs. E characteristic in the SCB model, when L_{fs} is adjusted so that the amplitude of the voltage spike agrees with the experimental value, it is found that dI_{fs}/dt also coincides with the experimental data, as shown in Figure 8. (Actually, dI_{fs}/dt is relatively insensitive to the choice of L_{fs} .) Since the simulation predicts V_C fairly accurately, such adjustment of L_{fs} can be used to determine L_{fs} . The value 160 nH shown in Figure 7 was used for all the results given in this report. The switch resistance R_{ON} in Figure 7 does have a small effect. It was adjusted to the indicated value of 140 m Ω to optimize the firing set model.

Shot #1322 used a 10.34 μ F capacitor charged to 90 V. The initial energy E_o is 41.9 mJ, much more than that required to vaporize the bridge. The burst time predicted by the simulation is close to the experimental result, but the model predicts a very large value for dI_{fs}/dt , which results in a predicted voltage spike that is much too large—over 700 V. This will be discussed further below.

Shot #1334 used a 3.38 μ F capacitor charged to 50 V. The initial energy is 4.23 mJ, which in this case is just two to three times more than that required to vaporize the bridge. Again, the burst time predicted by the simulation is close to the experimental result. However, we believe that in this case, the model is at the lower end of the range of energies for which it is useful.

Shot #1335 used a 3.38 μ F capacitor charged to 28 V. The initial energy is 1.33 mJ in this case, less than the theoretical value required to vaporize the bridge. As it must, the model predicts that the bridge will not burst (see Figure 5). Experimentally, however, the bridge *does* burst; the burst time is about 5 μ s. This is an extremely important result. We believe that it is indicative of thermal feedback resulting from the ignition and burning of the explosive powder; this subject will be dealt with in the next section.

III. Behavior and Modeling of SCB Detonators Over a Broad Range of Energies

The results of the previous section show that a straightforward application of the methods used to model EBWs does not result in an SCB model that yields accurate results over a wide range of capacitor discharge unit (CDU) energies. In this section, we will present experimental data over such a range and discuss the results with a view toward developing a more robust model.

Experimental Data

In Figure 9, we show the R vs. E curves for a large number of shots. All of the data were taken with the same test configuration as for Figure 8. In all cases, the detonator fired; the SCB resistance begins to increase at the time of firing.

It is clear that the resistance is far from a unique function of the energy. The tests tend to fall roughly into three groups. (1) High-energy shots, for which the resistance rises fairly slowly with increasing energy after encountering the initial increase signaled by the beginning of the current drop, and rises rapidly at some higher energy; (2) Low-energy shots, for which the resistance starts to exhibit the usual rise and fall, and then suddenly makes a sudden rapid jump at burst; and (3) Intermediate-energy shots, which comprise a transition region between the previous two, but exhibit behavior similar to those at high-energy. Shot #1318, which was singled out above as exhibiting “classic” behavior, falls in the intermediate-energy region. The designation of the grouping into low, intermediate, and high energies applies not only to the electrical energy delivered to the SCB leads, which is the energy variable used as the abscissa of the plot in Figure 9, but also to the energy initially stored on the CDU. With the exception of Shot #1391 at 47.6 mJ CDU energy, all the shots to the left of #1318 (and #1317, which is identical to #1318), have lower initial CDU energy than the 23.9 mJ of #1318. Conversely, all the shots to the right of #1318 have higher initial CDU energy.

Another view of the data from these shots is given in Figure 10, which shows burst times as a function of the energy at burst. This accentuates the distinction between the low-energy and the intermediate- and high-energy regimes. The low-energy data exhibits a longer time to burst, as expected, and it tends to fall on a straight line as a function of energy. In the other two energy regimes, burst time does not vary with energy nearly as rapidly.

These results show that the simple SCB model discussed above, which is based on a unique expression of resistance as a function of energy, cannot provide accurate results over a wide variation of firing set parameters. We turn now to a discussion of procedures for modeling the SCB detonators which extends the validity of the model over the indicated energy ranges.

Modeling the SCB in the High-Energy Regime

Consider the high-energy data in Figure 9. The energy to burst tends to increase as the initial voltage on the CDU is increased. Furthermore, as the voltage is increased,

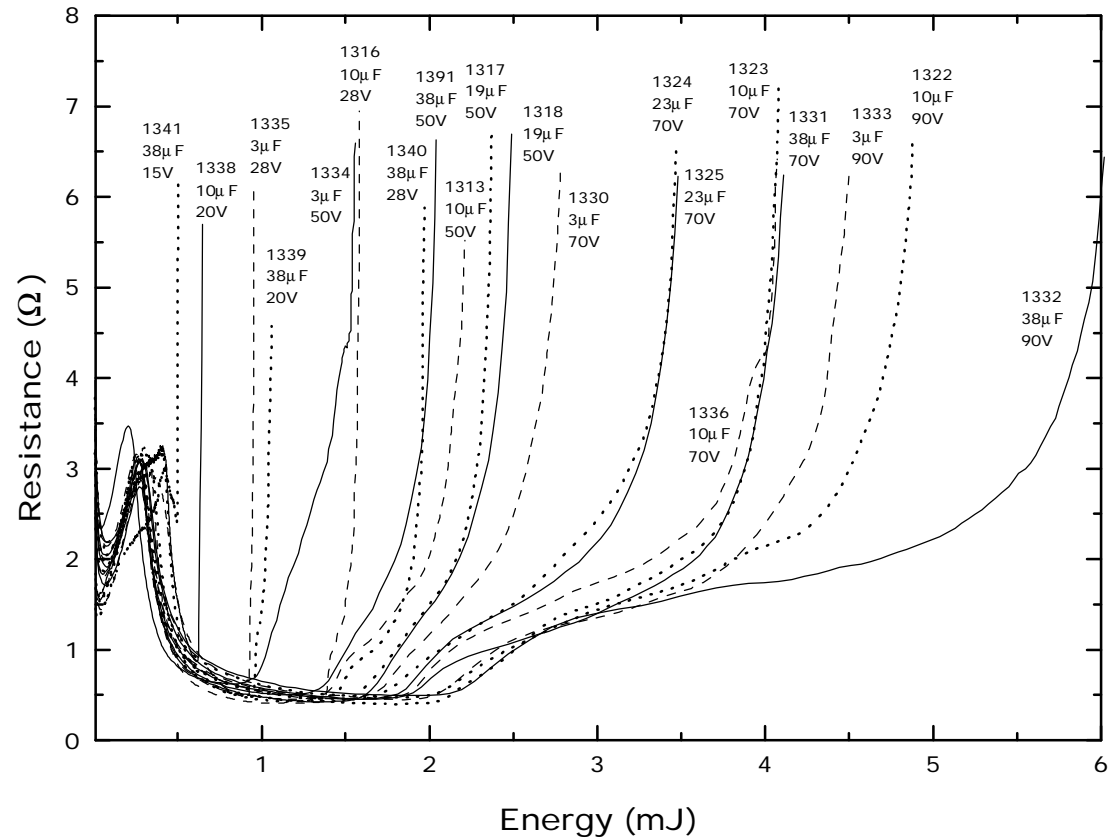


Figure 9. Resistance vs. energy for SCB shots ranging over a variety of CDU capacitances and initial voltages. The legends indicate shot numbers, capacitance to one or two significant figures, and voltage. Note that Shots 1317 and 1318, 1323 and 1336, and 1324 and 1325 represent pairs of shots with nominally identical conditions. This repetition was done to investigate shot-to-shot variation.

there is a stretching out of the energy required to vaporize the SCB and bring it to the point of very rapidly increasing resistance. We believe this behavior results from an energy loss mechanism. Naturally, there are losses in the SCB—for example, there will be ohmic losses in the leads and lands, and heat transfer from the bridge to the substrate, lands, and explosive powder. However, we cannot say whether the apparent energy loss is related to these particular phenomena.

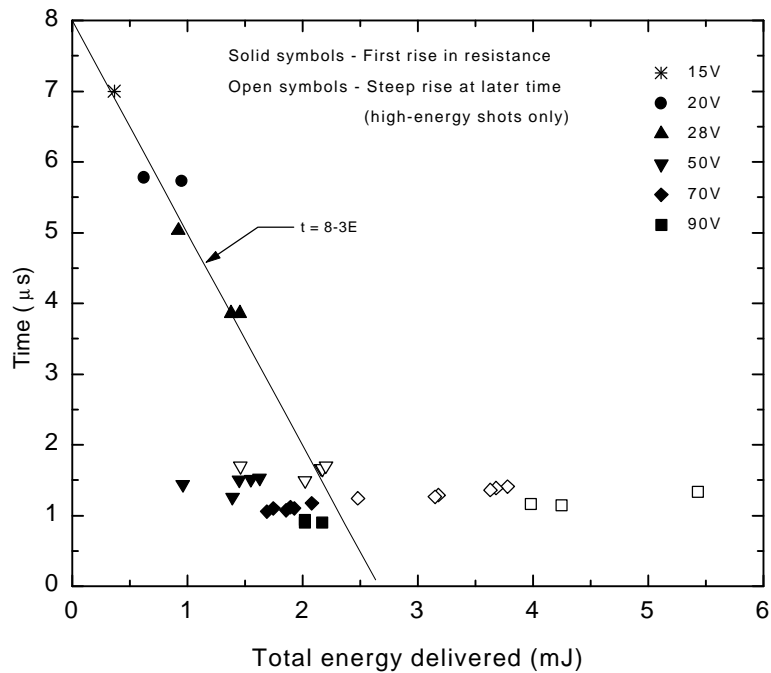


Figure 10. Burst times for data shown in Figure 9. The straight line is just an approximate fit to the low-energy data points; its formula $t=8-3E$ has no known physical significance. The solid symbols identify the first rise in resistance, which is defined as the burst time for the purposes of this report. The open symbols represent a semiquantitative estimate of the energies and times at which the resistance reaches a high value (5-7 ohms), and the R vs. E plot acquires a steep slope. Progression from left to right at any given voltage is roughly in order of increasing capacitance.

The fact that the loss appears to increase with CDU voltage suggests that it can be modeled by assuming that there are loss mechanisms which are an increasing function of voltage. Since there is no reason to believe that the loss mechanisms remember the initial voltage that the SCB sees, the most straightforward approach is to assume that the loss is a function of the instantaneous voltage V at the SCB leads. This suggests that the SCB energy budget might be described by the following equation:

$$\frac{dE_{SCB}}{dt} = VI[1 - A_L f_L(V)] \quad (5)$$

where E_{SCB} is the instantaneous energy contained in the bridge itself, $f_L(V)$ is a function of instantaneous SCB voltage used to define the functional form of the loss, and A_L is a multiplicative constant used to adjust the amplitude of the loss. Since the data in Figure 9 offer no way to determine whether the loss mechanism manifests itself at low voltage, we use a function $f_L(V)$ that is zero at low voltages. The function we chose that satisfies this criterion and that increases as a function of voltage is shown in Figure 11. It must be emphasized that this choice has no physical basis. Consideration of the data simply indicates that it is qualitatively plausible. (In particular, it should be noted that if heat transfer from the SCB to the surroundings is responsible for the apparent energy loss, it must be a nonlinear phenomenon, because one would expect linear heat transfer to be most effective when the time scales are long, rather than in the high-energy case when they are short.)

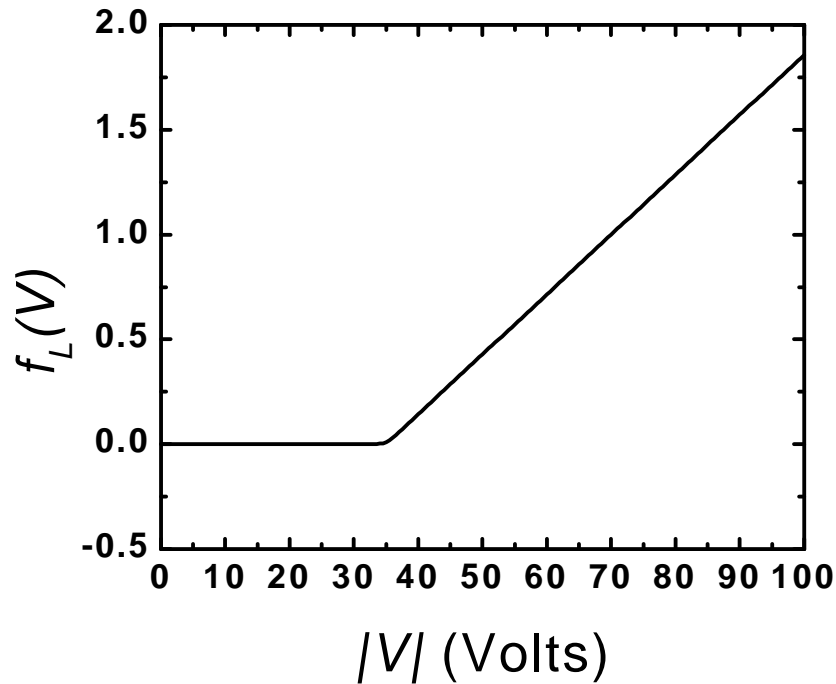


Figure 11. The function $f_L(V)$ of SCB voltage which is used in the energy loss model. It consists of two straight lines connected by a smoothed transition at the corner. Note that the absolute value of voltage is used, so that the model does not depend on polarity.

We adopt the point of view that shot #1318 (in the intermediate energy range) exhibits something like the R vs. E behavior that one would expect from an SCB with no

losses, i.e., that the resistivity is the unique function of specific energy that one would expect from a thermally isolated sample of the polysilicon used. This is to be regarded as only a working supposition. There is no reason to believe that losses in Shot #1318 are negligible. We therefore assume that the SCB resistance is given by the same tabular fit to the R vs. E data from Shot #1318 as was used in the simple model. However, we now integrate Eq. (5) to obtain the SCB energy, rather than simply integrating the power VI with respect to time, as was the case in the simple model (i.e., $A_L=0$). From Figure 8, we see that, in Shot #1318, the SCB voltage was approximately 35 V prior to burst. This is the reason for the choice of 35V as the transition voltage for $f_L(V)$; at higher voltages the loss term will become active.

For practical purposes, it is important to note that the use of two straight lines with a sharp corner in this model sometimes results in nonconvergence of a PSpice computation. This problem was solved by including a narrow transition region to mate the two lines at the corner. We used a circular arc extending for one volt on each side of the 35 volt transition voltage.

Given the function $f_L(V)$, we must determine the multiplicative constant A_L . We chose to adjust A_L so as to obtain the best fit to the data from the high-energy Shot #1322, for which the firing set capacitance was 10.34 μF and the CDU voltage was 90 V. These parameters represent the nominal capacitance but the maximum voltage anticipated for our applications. Hence, we will be interpolating in voltage and extrapolating to capacitance values on either side of 10 μF . We found that the value $A_L=0.3$ gives a remarkably good fit to the voltage and current data from Shot #1322. The results are shown in Figure 12; this data from the model with the loss term can be compared with the results of the simple model shown in Figure 8.

There is very little difference between the lossy model and the simple model for shot #1334, as the voltage is sufficiently low that the loss term has little effect. The results for Shot #1335 are no different at all from those shown in Figure 8, because the voltage never reaches the transition voltage of 35 V. We see that the behavior of the model after burst time has deteriorated somewhat for Shot #1318, but up to that point it is still quite good. The behavior of the lossy model for shots #1334 and #1318 are similar in that the burst times are somewhat greater than the experimental values and the voltage spikes are reduced.

In Figures 13 and 14, we show the results of applying this model to 18 of the 20 shots shown in Figure 9. Note that this is a blind test of the model for all shots except #1318 and #1322. It is seen that the model works best at high energies. Its performance deteriorates at low energies, but this is expected, as nothing has been put into the model up to this point to account for the deviation from “classic” behavior which is seen at low energies.

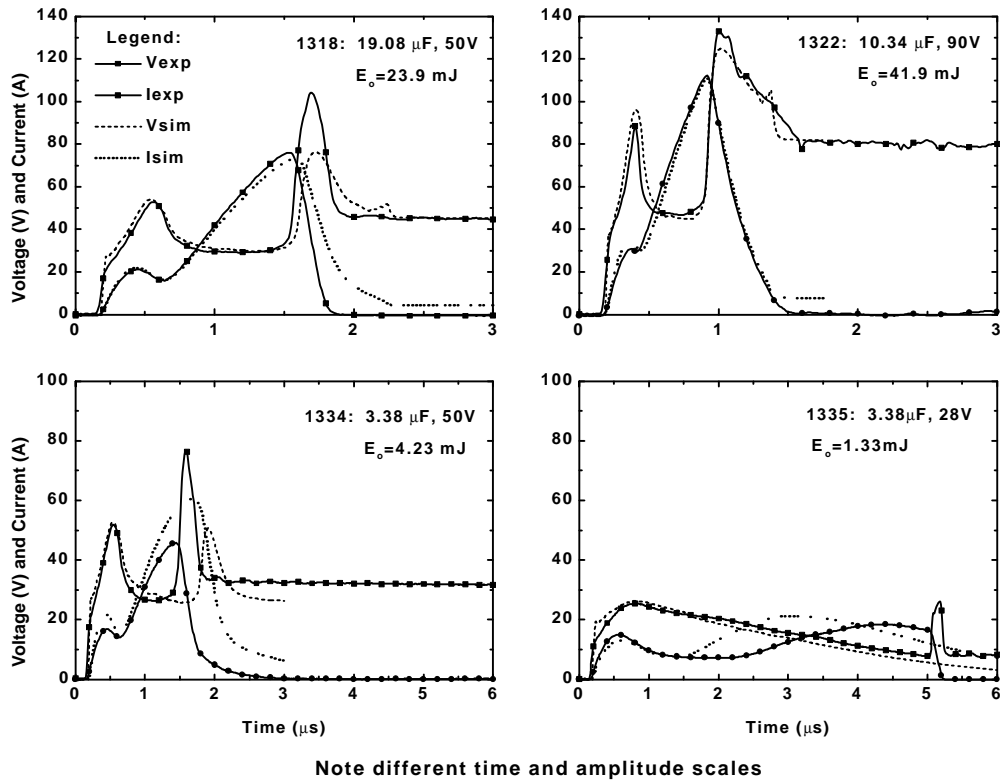
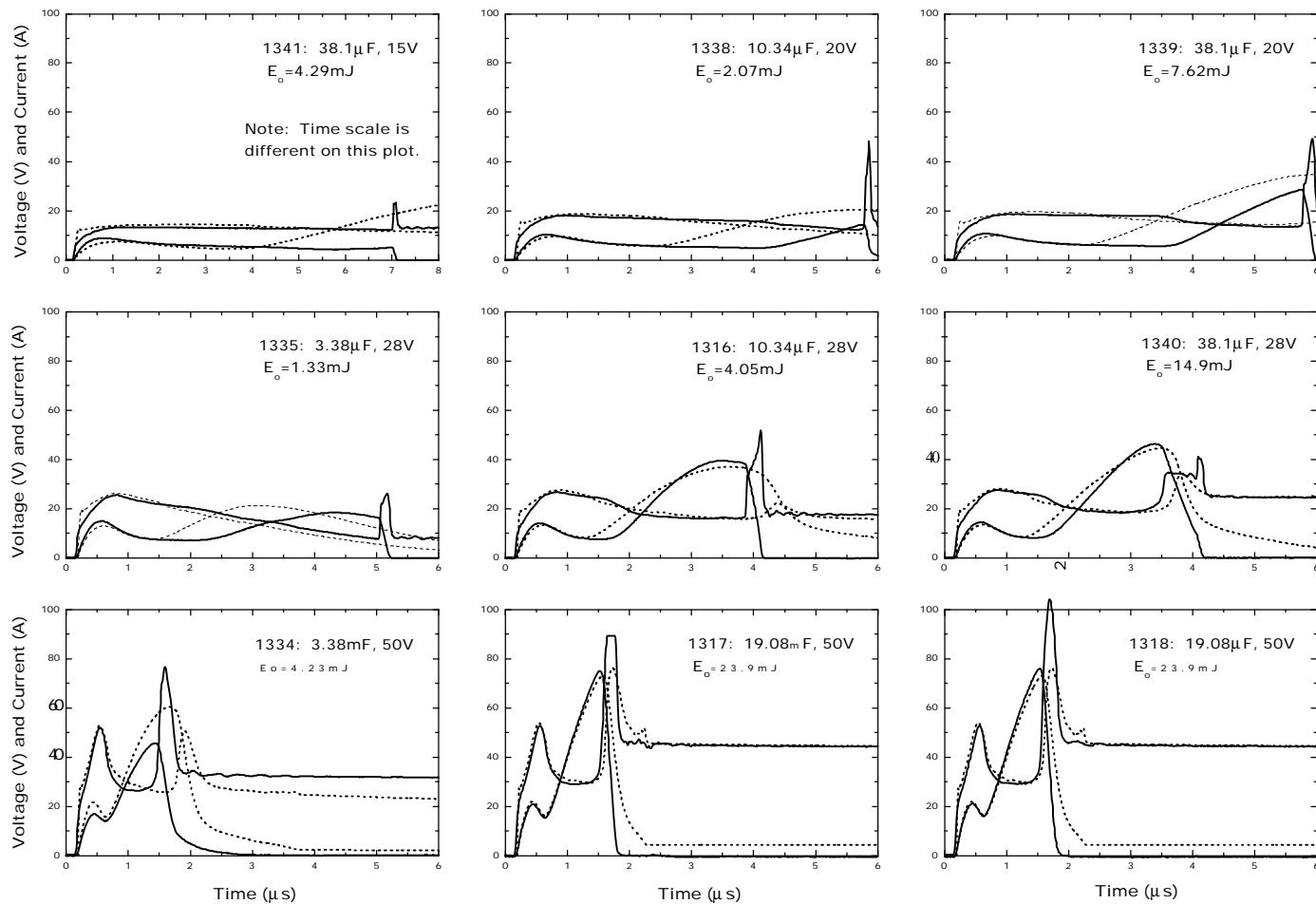


Figure 12. Results of applying the SCB model with the high-energy loss term to selected shots. Compare these plots to those in Figure 8.

As pointed out in the caption for Figure 9, Shots 1317 and 1318, 1323 and 1336, and 1324 and 1325 represent pairs of shots with nominally identical conditions. Note that the degree of shot-to-shot variation can be observed in greater detail in the experimental current and voltage data of Figures 13 and 14. It can be seen that the variation is not excessive for these shots.

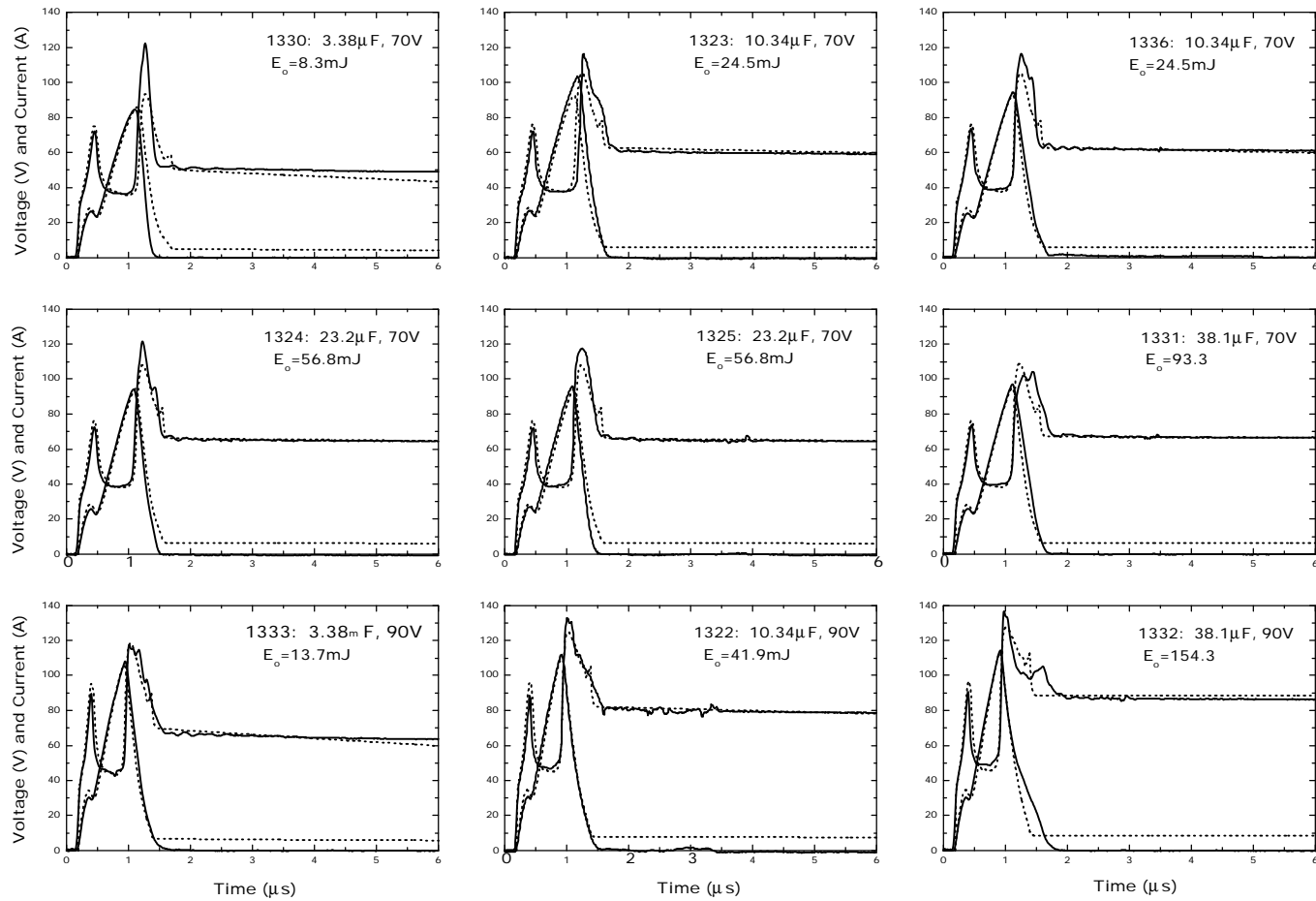
Modeling the SCB in the Low-Energy Regime

We now turn to the low-energy data in Figures 9 and 10 and the upper plots in Figure 13. As noted above, the detonators will often fire even though the initial energy stored on the CDU is less than the energy required to completely vaporize the SCB. By “often” we mean that they fire for a variety of capacitance and voltage values, not that they fire unreliably for given capacitance and voltage values. Clearly, for sufficiently low voltage at any given capacitance, a point will be reached when they no longer fire



Note vertical scale 0-100

Figure 13. Data from nine SCB shots in the low and intermediate energy range (solid lines), and the results of simulations of these tests with the lossy SCB model (dashed lines).



Note vertical scale 0-140

Figure 14. Data from nine SCB shots in the high energy range (solid lines), and the results of simulations of these tests with the lossy SCB model (dashed lines).

reliably, or do not fire at all. But that point was not reached in the series of experiments portrayed in Figures 13 and 14.

Another feature of the low-energy data is that, while the SCBs take longer to burst as the energy and voltage on the CDU are decreased, they burst very suddenly when they do burst. We are indebted to Prof. K. C. Jungling (Jungling, 1996) for pointing out that a reasonable explanation for both these characteristics is that, as the SCB heats up and perhaps starts to vaporize, the explosive powder ignites and burns, feeding heat back into the SCB and completing the vaporization process in the bridge.

We developed a model based on this supposition. What follows is an outline of the derivation of the model; a more detailed development is given in Appendix A. We assumed that the powder will ignite after it “cooks” for some period of time and that a quantitative description of this “cooking” is simply the thermal energy transferred from the SCB to the powder. We assumed that the rate of heat transfer can be described by the simple equation

$$\frac{dE_p}{dt} = h_p(T_{SCB} - T_p) \quad (6)$$

where E_p is the energy transferred into the powder, T_{SCB} is the temperature of the SCB, T_p is the temperature of the powder, and h_p is a heat transfer coefficient. We then made the assumption that the specific heat of the polysilicon is constant (a poor assumption), and that the powder temperature that matters in the heat transfer equation is the temperature of the unheated powder. Then Eq. (6) can be written

$$\frac{dE_p}{dt} = H_p E_{SCB} \quad (7)$$

where H_p is a new heat transfer coefficient assumed to be constant.

We assumed that the powder ignites when E_p reaches some fixed value E_{PI} . The form of Eq. (7) is such that only one independent parameter E_{PI}/H_p need be determined. We then develop an equation for heat transfer back into the SCB along the lines of that used to go from Eq. (6) to Eq. (7) and write the transfer rate as

$$\left[\dot{E}_{SCB} \right]_{TF} = H_{SCB} (E_{PB} - E_{SCB}) \quad (E_p \geq E_{PI}) \quad (8)$$

where E_{PB} is a constant which is a measure of the temperature of the burning powder, H_{SCB} is another heat transfer coefficient (assumed constant), and the subscript TF on the heating rate stands for “thermal feedback”, the term we will use to describe this process.

Note that this is very approximate and based on rather qualitative arguments. As noted above, this approach essentially assumes that the specific heats are constant, although this is not true for polysilicon, (Martínez Tovar, 1993). The assumption that E_{PI}/H_p , H_{SCB} , and E_{PB} are constants that are applicable over a wide range of conditions is tenuous. However, because of the complexity of the processes and the number of unknown quantities involved, we are forced to overlook these objections and to use qualitative ideas to derive a workable but approximate model.

Adding the heat transfer due to thermal feedback to energy equation (5), we obtain a revised model in the form

$$\frac{dE_{SCB}}{dt} = VI[1 - A_L f_L(V)] + \left[\dot{E}_{SCB} \right]_{TF}. \quad (9)$$

The implementation of the complete SCB model in a PSpice library is given in Appendix B.

The R vs. E table from Shot #1318 which was used above in the simple model and in the lossy model does not give good results when applied with Eq. (9) to the low-energy shots. The reason is that at early times, the SCB resistance in Shot #1318 is too low (see Figure 15). This results in a deposition of energy in the SCB which is too rapid, so that there is an early resistance drop and current rise in the simulation. This problem was addressed by considering three shots which range from very low energy up to the midrange in energy (Shots #1338, #1316, and #1318). A new R vs. E table was created by drawing the curve plotted as solid squares in Figure 15 that follows the data from #1338 at first, then switches to #1316, then switches to #1318.

The parameters $E_{PI}/H_p = 1.9$ ns, $H_{SCB} = 0.5$ MHz, and $E_{PB} = 10$ mJ were chosen by trial and error to obtain a reasonably good simulation of Shots #1338 and #1316. Results from applying the model with these parameters to the all of the tests discussed previously are shown in Figures 16 and 17. These simulations constitute a blind test of the model except for shots #1338, #1316, #1318, and #1322. As expected, the thermal feedback model results in a significant improvement in the agreement between simulation and experiment in the first five shots (the lowest-energy shots) in Figure 16.

However, note that the model predicts a drop in voltage at the time of powder ignition for Shots #1341, #1338, and #1339. The reason for this is that, at that time for those shots, the slope of the R vs. E curve is negative. Hence, the influx of energy from the powder results in an initial drop in resistance before the occurrence of the resistance rise associated with burst. This sharp drop in voltage is not observed in the experimental data from those three shots. Rather, the sharp rise in voltage is preceded by a slight and gradual drop in voltage, some of which can be attributed to the discharge of the CDU. This illustrates a quantitative inaccuracy of the model.

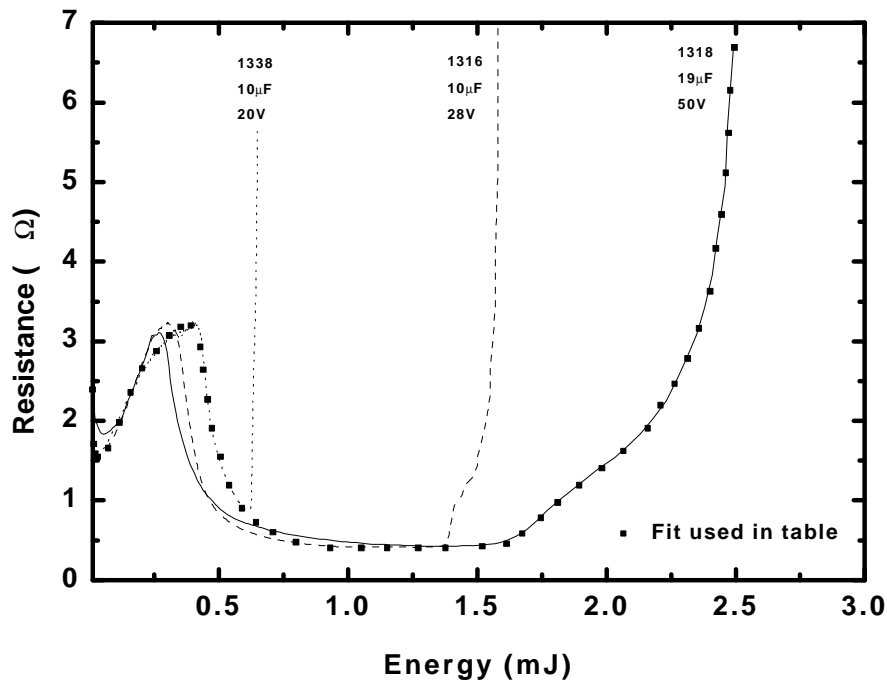


Figure 15. Data from three shots varying from the low to intermediate energy regimes. The square symbols indicate the data used to obtain a composite fit for the SCB model (see text).

The agreement between simulation and experiment in the intermediate- and high-energy ranges in Figures 16 and 17 is not quite as good as for the model in which thermal feedback was omitted (see Figures 12-14). The reason for this is that the new R vs. E table (see Figure 15) does not match the experimental data as well as that obtained from Shot #1318 alone. Still, for high energy shots, the simulation results are less sensitive to the details of the early-time resistance behavior than are those for low energy shots. Hence, the model which combines thermal feedback with the nonlinear energy loss does a fairly good job over the entire data range.

The thermal feedback mechanism always causes a large voltage spike at powder ignition. It is of interest to observe that some of the intermediate and high energy data exhibits a late-time voltage spike that could be interpreted as powder ignition. This is particularly noticeable in Shot #1332, but is present in some of the other shots as well.

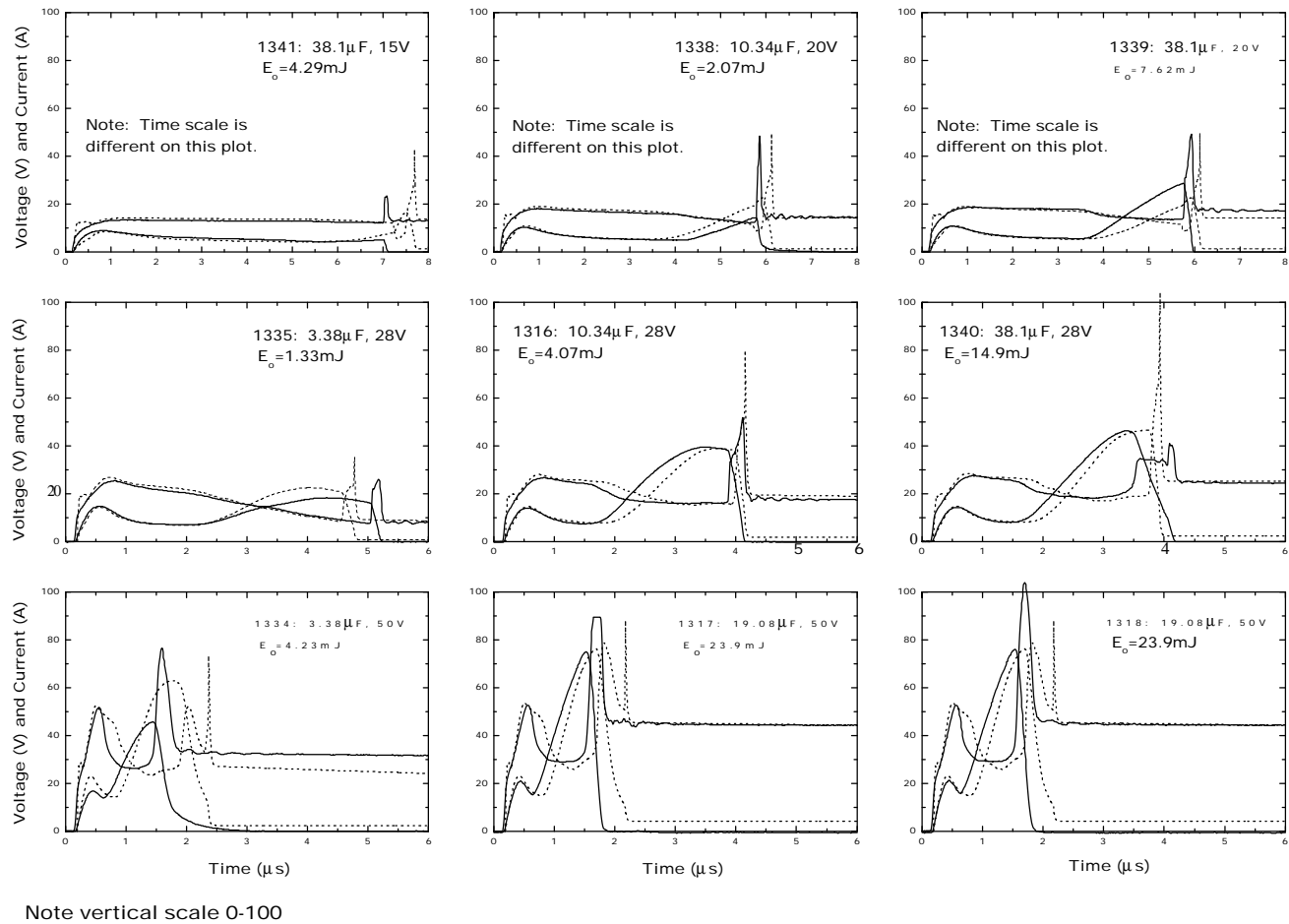
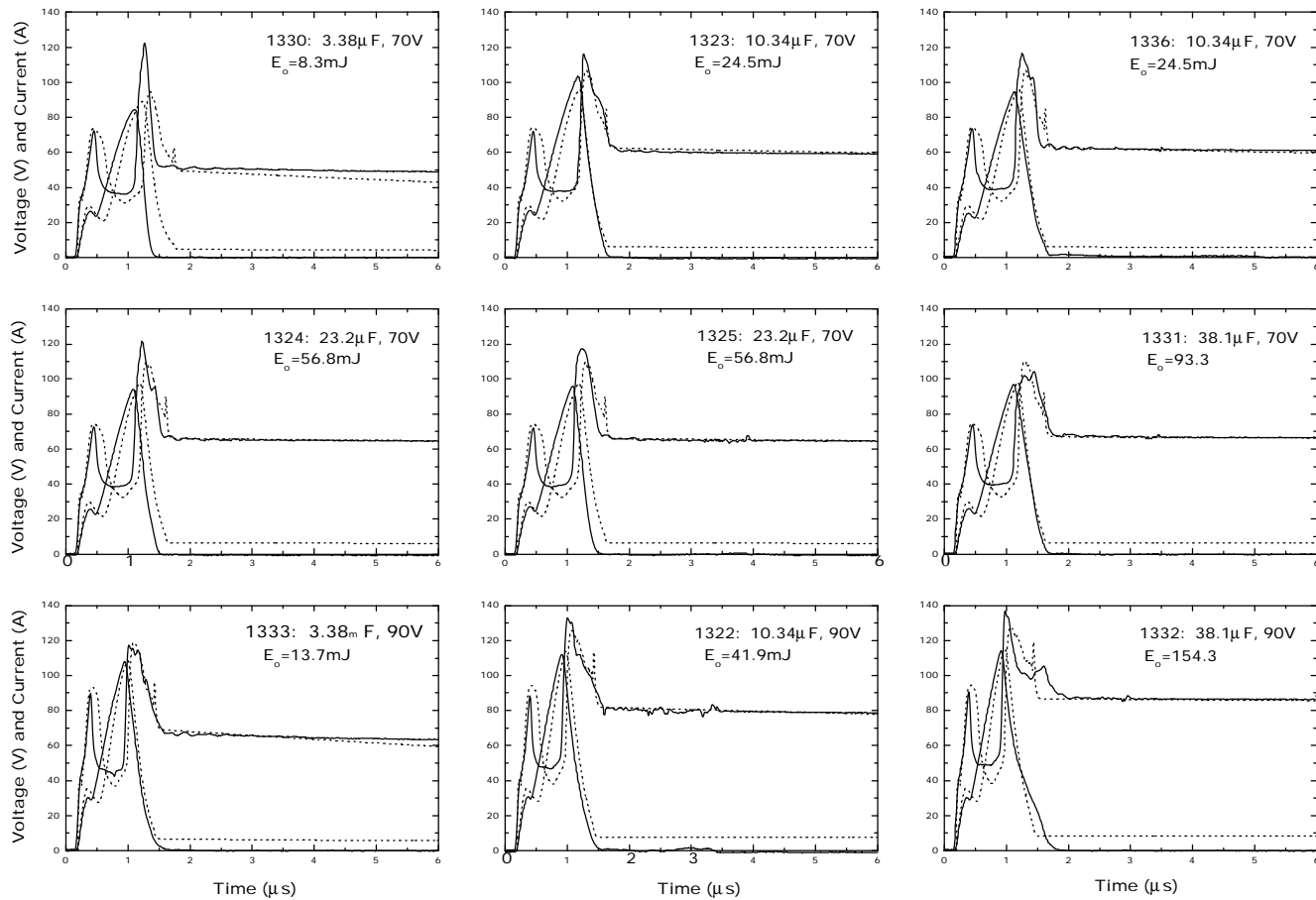


Figure 16. Data from the nine SCB shots in the low and intermediate energy range shown in Figure 13 (solid lines), and the results of simulations of these tests with the thermal feedback SCB model (dashed lines).



Note vertical scale 0-140

Figure 17. Data from the nine SCB shots in the high energy range shown in Figure 14 (solid lines), and the results of simulations of these tests with the thermal feedback SCB model (dashed lines).

Tests of the Models in A Different Configuration

As a test of the models developed above, they were applied to simulations of some shots fired with a slightly different configuration. (Because the differences are slight, this is admittedly a relatively mild test.) Instead of the very short wires connecting the detonator to the firing set, in these tests the connection was made with 16 inches of RG-58 cable plus 6 inches of 22 gauge twisted pair wires (see the first four entries in Table I). This amount of additional connecting hardware makes a difference in shots fired at intermediate and high energy, in which the time scales are relatively short. However, it does not make a significant difference in shots fired at low energy, where the time scales are long and cable inductance is not so important.

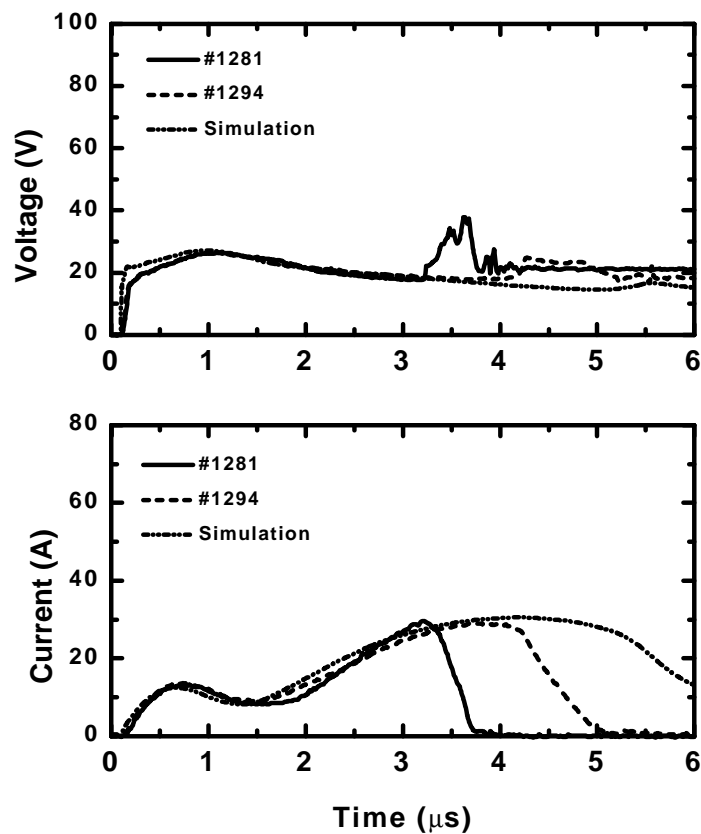


Figure 18. Simulation results using the lossy model *without* thermal feedback and experimental data from Shots #1281 and #1294. These tests were carried out with a capacitance of $9.57 \mu\text{F}$ and a CDU voltage of 28 V. The CDU energy E_c is 3.57 mJ. The detonator was connected to the firing set with 16 inches of RG-58 cable plus 6 inches of 22 gauge twisted pair wires.

Figure 18 shows data from two nominally identical low-energy shots and a simulation made with the lossy model without thermal feedback. Note that significant shot-to-

shot variation in the experimental data is seen—of the order of a microsecond difference in burst time. But in the absence of thermal feedback, the simulation does not predict burst at a time comparable to that of either of the two experiments. What is seen instead is a rather weak drop in current one or two microseconds later.

Figure 19 shows the same data with a simulation which includes thermal feedback (in addition to the nonlinear loss term, just as in the simulations discussed in the previous subsection). The simulation now predicts a burst time at about that of one of the shots (#1294). Data from the comparable shot #1316 made with the short connection from firing set to detonator is shown for comparison. It is seen that its burst time falls between the two; the extra cabling has little effect.

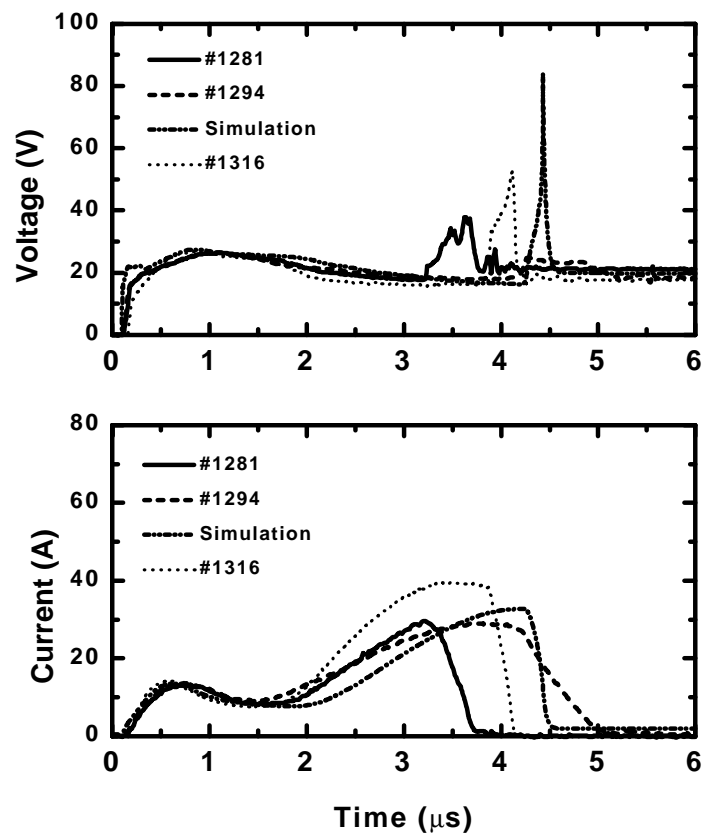


Figure 19. Simulation results using the lossy model *with* thermal feedback and experimental data from Shots #1281 and #1294 (see Figure 18). Data from Shot #1316 (using short connecting wires and a capacitance of $10.38 \mu\text{F}$, with $E_o = 4.07\text{mJ}$) is given for comparison.

Figure 20 shows data from two nominally identical intermediate energy shots, with a simulation made with the lossy model without thermal feedback. Again, significant shot-

to-shot variation in the experimental data is seen. Data from the comparable shot #1318 made with the short connection from firing set to detonator is shown for comparison. In this case, the extra cabling does affect the results—burst appears ahead of the long-cable data and the simulation. The addition of thermal feedback would not change the simulation results significantly, except for a sharp voltage spike appearing well after burst—see Shot #1318 in Figure 16.

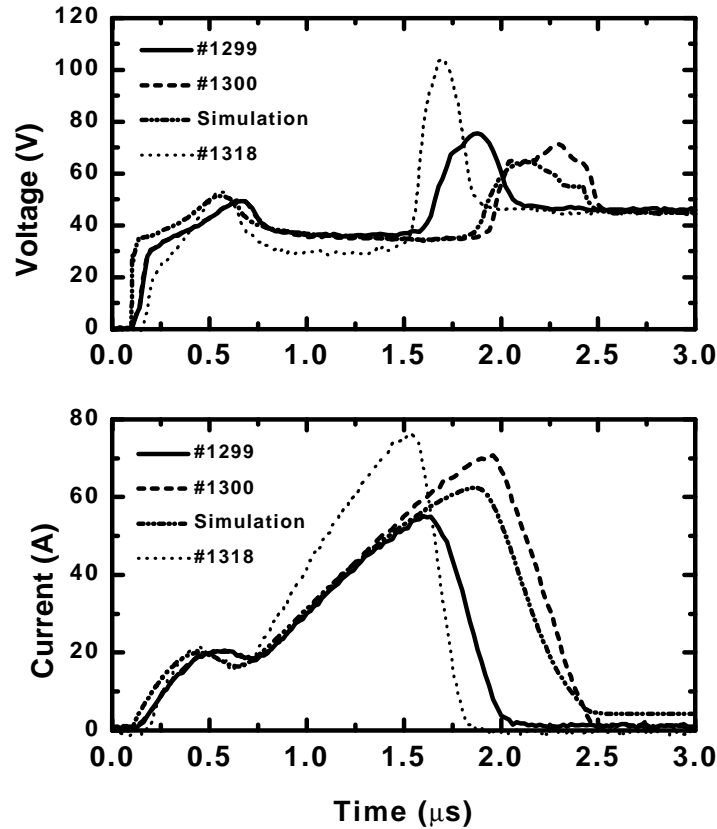


Figure 20. Simulation results using the lossy model *with* thermal feedback and experimental data from Shots #1299 and #1300. These tests were carried out with a capacitance of 19.08 μF and a CDU voltage of 50 V. The CDU energy E_o is 23.9 mJ. As for Shots #1281 and #1294, the detonator was connected to the firing set with 16 inches of RG-58 cable and 6 inches of 22 gauge twisted pair wires. Data from Shot #1318 (using short connecting wires, otherwise the same) is given for comparison.

IV. Conclusion

Data from detonators using semiconductor bridges as initiators and BNCP as the explosive powder have been presented. The data show that these SCB/BNCP detonators can be electrically characterized by assuming that their resistance is a function of the energy deposited in the bridge, but only after accounting for an energy loss and the feedback of thermal energy from the burning explosive powder.

The energy loss is only apparent in the data; it has not been positively identified as originating from any particular mechanisms. It appears to be a nonlinear function of the voltage across the SCB terminals and is important only at the higher voltage levels of SCB operation. One of the SCB models used in this report, referred to as the lossy model, uses a specification of the resistance as a function of SCB energy, with the energy budget determined by subtracting an empirically derived nonlinear loss term from the electrical power flowing into the SCB terminals.

The thermal feedback mechanism is most important at the lower levels of energy stored in the CDU. A model for it is derived from some very approximate arguments for heat transfer, first to heat the powder to the point of ignition, and then to include the transfer of thermal energy back into the SCB in the SCB energy budget. The addition of this mechanism to the lossy model results in an overall model referred to as the thermal feedback model. In this model, it was found useful to modify the resistance versus energy profile to reflect the slightly different behavior observed at low and high voltage levels.

Our recommendation is to use the lossy model without thermal feedback for simulations of detonator systems for which operation is clearly in the high energy range. But the thermal feedback model with the revised R vs. E table should be employed in any simulation in which the energy supplied to the detonator is considered to be marginally sufficient for firing. This use of different models in different voltage/energy regimes has a precedent in the simulation of systems employing EBWs, where different models are used depending on the current expected at burst.

The models derived here have been shown to give useful results when applied to simulations of various detonator experiments. However, the models should be subjected to more extensive tests in simulations of more complex practical explosive systems to better define their limitations and to provide data for their improvement.

Acknowledgments

We would like to thank the following for many useful discussions and for their support during the completion of this project: Prof. Ken Jungling (UNM), Bernardo Martínez Tovar (SCB Technologies, Inc.), Rene Bierbaum, Mike Deveney, Carl Furnberg, Steve Harris, Bob Oetken, and Jamie Stamps (all Sandia).

References

Benson, D. A., Larsen, M. E., Renlund, A. M., Trott, W. M., and Bickes, R. W., Jr., "Semiconductor bridge: A plasma generator for the ignition of explosives," *J. Appl. Phys.* **62** (5), 1662 (1987).

Bickes, R. W., Jr., Schlobohm, S. L., and Ewick, D. W., "Semiconductor Bridge (SCB) Igniter Studies: I: Comparison of SCB and Hot-Wire Pyrotechnic Actuators," 13th International Pyrotechnics Seminar, Grand Junction, CO, July 11-15, 1988.

Bickes, R. W., Jr., Grubelich, M. C., Harris, S. M., Merson, J. A., and Weinlein, J. H., "An Overview of Semiconductor Bridge, SCB, Applications at Sandia National Laboratories," Sandia National Laboratories Report SAND95-0968C (1995).

Furnberg, C. M., "Computer Modeling of Detonators," IEEE 37th Conference on Circuits and Systems, Lafayette, Louisiana, August 3-5, 1994.

Jungling, K. C., private communication (1996).

Martínez Tovar, B., "Electrothermal Transients in Highly Doped Phosphorous Diffused Silicon-on-Sapphire Semiconductor Bridges (SCB) Under High Current Density Conditions," Ph.D. Dissertation, The University of New Mexico, Albuquerque, New Mexico, July, 1993.

Appendix A

In this appendix, we provide details of the derivation of Equations (7) and (8) for the thermal feedback mechanism. We assume that prior to powder ignition, the rate of heat transfer from the SCB to the powder can be described by the equation

$$\frac{dE_p}{dt} = h_p(T_{SCB} - T_p) \quad (6)$$

where E_p is the energy transferred into the powder, h_p is a heat transfer coefficient, T_{SCB} is the temperature of the SCB, and T_p is the temperature of the unheated powder (a constant). If the specific heat c_s of the polysilicon is constant, the SCB energy is

$$E_{SCB} = c_s T_{SCB} + E_{SCB}^0 \quad (A-1)$$

where E_{SCB}^0 is a constant which can be chosen arbitrarily, since the zero point of SCB energy is irrelevant. (Note: We could just as easily consider only the change in SCB energy ΔE_{SCB} and eliminate E_{SCB}^0 from the derivation. We have chosen the present approach simply because it seems natural to think of ignition at a certain energy *level*, viz., the value E_{PI} introduced below.) Defining a new heat transfer coefficient $H_p = h_p/c_s$ and making the choice

$$E_{SCB}^0 = -c_s T_p \quad (A-2)$$

Equation (6) becomes

$$\frac{dE_p}{dt} = H_p E_{SCB}. \quad (7)$$

Now assume that the powder ignites when E_p reaches some fixed value E_{PI} . Let the time at which this occurs be denoted t_{PI} . It can be determined by integrating Equation (7) from $t=0$ to $t= t_{PI}$. If H_p is assumed constant,

$$\frac{E_{PI}}{H_p} = \int_0^{t_{PI}} E_{SCB}(t') dt' \quad (A-3)$$

Note that only one independent parameter E_{PI}/H_p need be defined to obtain t_{PI} .

We now develop an equation for the heat transfer back into the SCB along the lines of that used to go from Eq. (6) to Eq. (7). The first step is to write the transfer rate as

$$\left[\dot{E}_{SCB} \right]_{TF} = h_{SCB} (T_{PB} - T_{SCB}) \quad (\text{A-4})$$

$$\begin{aligned} &= h_{SCB} \left[T_{PB} - \left(\frac{E_{SCB} - E_{SCB}^0}{c_S} \right) \right] \\ &= \frac{h_{SCB}}{c_S} [c_S T_{PB} + E_{SCB}^0 - E_{SCB}] \end{aligned} \quad (\text{A-5})$$

where h_{SCB} is a new heat transfer coefficient and T_{PB} is the temperature of the burning powder. Consistent with our previous crude approximations, we assume that h_p and T_{PB} are constants. It is to be understood that Equation (A-4) applies only after $t \geq t_{PI}$. Since E_{SCB} is always positive, this is the same as $E_p \geq E_{PI}$. Defining another heat transfer coefficient $H_{SCB} = h_{SCB}/c_S$ and a “burning powder energy” parameter

$$E_{PB} = c_S T_{PB} + E_{SCB}^0 \quad (\text{A-6})$$

we obtain the desired formula

$$\left[\dot{E}_{SCB} \right]_{TF} = H_{SCB} (E_{PB} - E_{SCB}) \quad (E_p \geq E_{PI}). \quad (8)$$

Appendix B

The following is a netlist of a PSpice subcircuit for the SCB model (an asterisk in the first column denotes a comment in PSpice).

```
*****  
*****
```

* This is the SCB model which implements both the nonlinear loss term and the thermal
* feedback model. It is intended for use only for detonators using SCBs of type 3-2b1+
* with BNCP explosive powder pressed into TO46/Brass shells at 25 kpsi.

* Aloss is the loss coefficient A_L , delta is the size of the loss function transition
* region in Volts, V01 is the SCB voltage at the transition region, EpioHp = E_{PI} / H_P ,
* Hscb = H_{SCB} , Epb = E_{PB} .

```
.Subckt SCB_LE 1 2 Params:  
+ Aloss=0.3 delta=1.0 V01=35.0  
+ EpioHp=1.9n Hscb=0.5Meg Epb=0.01
```

* Vmon is just a current monitor. The SCB current I is I(Vmon).

```
Vmon 1 5 0
```

* V(101) is the energy E_{SCB} contained within the SCB itself. It is obtained by combining
* the sources and losses described below and integrating the result. (The sources and
* losses are represented as current sources charging or discharging a unit capacitance.)

* Gpower is the electrical power VI delivered to the det leads. Some of this energy is
* deposited in the semiconductor material (V(101)) and some is lost through Gloss.

```
Gpower 0 101 Value = {IF(TIME < .1p, 0, I(Vmon) * V(5,2)) }
```

* Gloss is thermal energy lost to the substrate, aluminum lands, explosive powder,
* etc. via the $A_L f_L(V)$ term in Equation (5). Note minus sign in front of Aloss denoting
* loss.

* The third line in the formula for Gloss is the value of the loss function $f_L(V)$ for SCB
* voltages between V01-delta and V01+delta. It is evaluated on a circular arc in
* (f, V/V01) space.

```
Gloss 0 101 Value = {IF(TIME < .1p, 0, -Aloss*IF(V(202) < V01-delta, 0.0 ,  
+ IF(V(202) > V01+delta, V(202)/V01-1.0,  
+ (3.*delta-sqrt(9.*delta*delta-(V(202) -V01+delta)*(V(202) -V01+delta)))/V01
```

```
+ ))
+ *I(Vmon)*V(1,2)
+ )}
```

- * Eabs is the absolute value of the voltage at the SCB input leads. A separate voltage source is used to evaluate it only to avoid repetition of the term $\text{abs}(V(1,2))$ in Gloss.
- * Rabs is just a resistor to complete the circuit.

```
Eabs 202 0 Value={abs(V(1,2))}
Rabs 0 202 1.0T
```

- * Gpwr is the rate at which energy is fed back into the SCB by the powder (see Equation (8). Note that $V(201)$ is the integral of Gignit.

```
Gpwr 0 101 Value = {IF(TIME < .1p, 0,
+ IF(V(201) > EpioHp, Hscb*(Epb-V(101)) , 0)
+ )}
```

- * Cenergy is the unit capacitance used to integrate the power to obtain energy deposited in the SCB. Renergy is just a leakage resistor.

```
Cenergy 101 0 1
Renergy 101 0 1E12
```

- * $V(201)$ is a marker used to determine if the powder has ignited.
- * Gignit is the source for the ignition marker. It is equal to the SCB energy E_{SCB} , so $V(201)$ is the integral of energy vs time (see Equation (A-3)).

```
Gignit 0 201 Value = { IF(TIME < .1p, 0, V(101))}
```

- * Cignit is the unit capacitance used to integrate to obtain the time at ignition. Rignit is just a leakage resistor.

```
Cignit 201 0 1
Rignit 201 0 1E12
```

- * Edet is a voltage source which provides the proper voltage V across the SCB. It is equal to the SCB current I times the SCB resistance R .

```
Edet 5 2 Value = { I(Vmon) * V(301) }
```

- * Eres is the SCB resistance R evaluated from the table of R vs E_{SCB} values.

```
Eres 301 0 TABLE { V(101) }
```

+ (-1000 , 5.06129)
 + (1.25E-6, 5.06129)
 + (2.5E-6, 3.95649)
 + (3.75E-6, 3.47432)
 + (5E-6, 3.08165)
 + (6.25E-6, 2.86042)
 + (7.5E-6, 2.74148)
 + (8.75E-6, 2.62254)
 + (1E-5, 2.50361)
 + (2.08333E-5, 1.58496)
 .
 .
 .

[Most of the entries in the table are not shown in the interest of brevity. Note that a different table was used for the thermal feedback model than was used for the lossy model alone. This was due to differences in the R vs E behavior of the SCBs at different energy levels (see main text).]

.
 .
 .
 + (0.0024, 3.52311)
 + (0.00242, 3.88895)
 + (0.00244, 4.34531)
 + (0.00246, 4.84931)
 + (0.00248, 5.75775)
 + (0.0025, 6.69085)
 + (0.002505, 9.00297)
 + (0.002510, 10.48473)

.Ends

Distribution:

- 1 Prof. K. C. Jungling, Chairman
Department of Electrical and Computer Engineering
University of New Mexico
Albuquerque, NM 87131-1356

- 1 B. A. Martínez Tovar
SCB Technologies, Inc.
1009 Bradbury Dr., SE
Albuquerque, NM 87106

- 1 C. B. McCampbell
Beecher, Inc.
Rt. 5, Box 5235
Albuquerque, NM 87123

- 1 TPL, Inc.
Att: R. L. Brown, D. Schaeffer
3921 Academy Pkwy North, NE
Albuquerque, NM 87109-4416

- 1 A. Kammerman,
K & V Scientific Co., Inc.
901 18th Street, Suite 21300
Los Alamos, NM 87544

- 1 The Ensign-Bickford Company
Att: L. J. Mecca, P. Marshall, D. W. Ewick
660 Hopmeadow Street
P.O. Box 483
Simsbury, CT 06070-0483

- 1 Thiokol Corporation
Att: W. B. Greeg, Jr., M. Kramer
P.O. Box 241,
55 Thiokol Road
Elkton, MD 21922-0241

- 1 Quantic Industries, Inc.
Att: K. Willis, M. Berrera
990 Commercial Street
San Carlos, CA 94070-4084

1 Robert W. Ingham
 Teledyne McCormic Selph
 3601 Union Road
 P.O. Box 6
 Hollister, CA 95024-006

1 R. W. Davis, LLNL, L-281
 1 R. S. Lee, LLNL, L-281

1 MS 0311 J. W. Hole, 2671
 1 MS 0328 J. A. Wilder, 2674
 1 MS 0457 J. S. Rottler, 2001
 1 MS 0481 M. M. Harcourt, 2167
 1 MS 0481 M. A. Rosenthal, 2167
 1 MS 0481 D. L. Thomas, 2167
 4 MS 0486 S. S. Kawka, 2123
 1 MS 0525 C. W. Bogdan, 1252
 1 MS 0525 M. F. Deveney, 1252
 1 MS 0525 P. V. Plunkett, 1252
 1 MS 0953 W. E. Alzheimer, 1500
 1 MS 0985 J. H. Stichman, 2600
 10 MS 1453 R. W. Bickes, Jr. 1553
 1 MS 1453 F. H. Braaten, Jr., 1553
 1 MS 1453 M. C. Grubelich, 1553
 1 MS 1453 S. M. Harris, 1553
 1 MS 1453 G. R. Peevy, 1553
 1 MS 1454 D. E. Wackerbarth, 1553
 1 MS 1454 L. L. Bonzon, 1554
 1 MS 1454 W. W. Tarbell, 1554
 1 MS 0328 J. H. Weinlein, 2674
 1 MS 9004 M. E. John, 8100
 3 MS 9202 R. L. Bierbaum, 8116
 1 MS 9202 H.-T. Chang, 8116
 1 MS 9202 C. M. Furnberg, 8116
 20 MS 9202 K. D. Marx, 8116
 1 MS 9202 D. S. Post, 8116
 1 MS 9202 J. F. Stamps, 8116
 1 MS 9101 R. I. Eastin, 8411
 1 MS 9101 K. R. Hughes, 8411
 3 MS 9106 R. E. Oetken, 8417
 1 MS 9106 J. L. Van De Vreugde, 8417

10	MS 9021	Technical Communications Department, 8815, for OSTI
1	MS 9021	Technical Communications Department, 8815/Technical Library, MS 0899, 4414
4	MS 0899	Technical Library, 4414
3	MS 9018	Central Technical Files, 8940-2